Conference Proceedings

Solar World Congress 2015
Daegu, Korea, 08 – 12 November 2015

Heat transfer in a porous absorber and in an insulated pipe for solar convective furnace system

Manish Sachdeva, Dheeraj Saini, Gajanand Saini and Laltu Chandra[1]

Indian Institute of Technology, Jodhpur (India)

[1]Correspondence: chandra@iitj.ac.in

Abstract

This paper deals with heat transfer analysis in sub-systems for a concept of solar convective furnace system. This system makes use of open volumetric air receiver for heat transfer to air, which is employed as working fluid. In this paper, experimental and numerical evaluation of transient heat transfer (a) in porous absorber and (b) in an insulated pipe is presented. This shows temperature development in absorber and the heating up of an insulated pipe with transport of hot air. Mathematical models to analyze one-dimensional heat transfer in porous absorber and insulated pipe are developed and solved using numerical techniques. The tool, thus developed, is validated using the corresponding experiments. Comparative analysis shows that the predicted and experimentally obtained transient temperature profiles are comparable for both these components. Variations of about 5-15% are observed between numerically and experimentally obtained values.

Keywords: *Absorber, insulated pipe, transient heat transfer, 1-D numerical analysis, experiment*

1. Introduction

In the concept of solar convective furnace the reflected radiation from a heliostat field is concentrated onto porous absorbers of an open volumetric air receiver (OVAR); see e.g. Hoffschmidt et al., 2003. The sucked atmospheric air through the pores of absorber extracts the generated heat from concentrated solar irradiance. The detailed design basis and evaluation of cylindrical absorber based OVAR is presented by Sharma et al, 2015a, 2015b. The obtained thermally mixed hot air at the OVAR outlet can be stored in thermal energy storage for various applications, like metal processing, see e.g. Patidar et al., 2015a, 2015b. The schematic of designed and installed solar air tower simulator (SATS) facility for evaluation of such a system is presented in Sharma et al. 2015a, 2015b. It is realized that the transfer of hot air through the piping system will result in its heating up-to the desired steady state. In other words, the piping system will attain thermal equilibrium with convected hot air for solar convective furnace system. Achieving this equilibrium state may take several hours, which is quite considerable. Besides, heat loss through insulation due to temperature difference between hot air and ambient starts with the operation of furnace system, Patidar et al., 2015a. This depends on pipe material and its thermal properties. Also, the increase in insulation temperature with time will enhance natural convective heat loss to ambient. It is to be emphasized that steady inlet temperature is desired process heat applications, like material processing. To reduce the required time for achieving steady-state, pre heating of sub-systems/components are required, see e.g., Vasiliev et al., 1987. In view of these observations following are presented in the paper:

a. Numerical and experimental evaluation of transient heat transfer in a porous absorber
b. Numerical and experimental evaluation of transient heat transfer from hot air to ambient in an insulated pipe.

Nomenclature

C_{pf}	*Specific Heat capacity of fluid (J/kgK)*	$\dot{Q}_{Nat.\ conv}$	*Rate of Natural Convective Heat transfer(W)*
C_{pins}	*Specific Heat capacity of insulation (J/kgK)*	$\dot{Q}_{stf}$	*Rate of Heat transfer from solid to fluid (W)*

doi:10.18086/swc.2015.04.03 Available at http://proceedings.ises.org

C_{ps}	Specific Heat capacity of pipe/absorber (J/kgK)	$\dot{Q}_{sti}$	Rate of heat transfer from solid to insulation (W)
D_a	Diameter of absorber(m)	r	radial coordinate of absorber/pipe
D_p	Diameter of each pore of absorber (m)	Ra	Rayleigh No.
$\dot{E}$	Electrical Power Input (W)	r_a	radius of absorber(m)
h_{ex}	Natural convective heat transfer coefficient(W/m^2K)	Re	Reynolds No.
h_f	heat transfer coefficient for internal heat transfer in fluid(W/m^2K)	r_p	radius of pore(m)
L	length of absorber (m)	r_{ins}	outer radius of insulation (m)
K_{ins}	Thermal conductivity of insulation(W/mK)	r_s	radius of solid pipe (m)
K_s	Thermal conductivity of pipe/absorber(W/mK)	t	time
n_p	no of pores	T	Temperature (K)
Nu_f	Nusselt number for fluid	T_a	Ambient Temperature (K)
Nu_{ex}	Nusselt number for natural convection	T_{inlet}	Temperature at inlet of absorber (K)
$\dot{m}_f$	mass flow rate(kg/s)	T_{ins}	Temperature of insulation (K)
Pr	Prandtl number	T_m	Mean Temperature of fluid (K)
$\dot{P}$	Power Transfer to pipe(W)	$T_{m,\,pipe\,inlet}$	Mean temperature of fluid at inlet of the pipe connecting the absorber
q''	heat flux on absorber radial surface (W/m^2)	$T_{m,\,pipe\,outlet}$	Mean temperature of fluid at the outlet of the pipe connecting the absorber
$\dot{Q}_{cond}$	Rate of Conductive Heat transfer (W)	T_{ra}	Temperature of air recirculating to the receiver(K)
$\dot{Q}_{fts}$	Rate of heat transfer from fluid to solid (W)	T_s	Temperature of pipe/absorber (K)
$\dot{Q}_{atp}$	Rate of heat loss to pipe from absorber during experiment (W)	z	z-coordinate (along pipe/absorber)

Greek Symbols

α_f	Thermal diffusivity of fluid (m^2/s)	ρ_{ins}	Density of insulation(kg/m^3)
α_{ins}	Thermal diffusivity of insulation (m^2/s)	ρ_s	Density of pipe/absorber (kg/m^3)
α_s	Thermal diffusivity of pipe/ absorber (m^2/s)	δ	Thickness of pipe (m)
$\emptyset$	porosity of absorber	Δl	Distance between any two thermocouples on insulation (m)

Abbreviations Used

OVAR	Open Volumetric air receiver	SATS	Solar Air tower Simulator
POA	Power on Aperture (W)	MFR	Mass flow rate (kg/s)

Subscripts Used

a	absorber/ambient	ins	insulation domain
avg	average	Inlet	Inlet of pipe/absorber
ex	external convection	p	Pores in absorber
f	fluid domain	s	solid domain
fd	fully developed length		

2. Transient heat transfer in porous absorber

As described, the developed concept of solar convective furnace concept is based on open volumetric air receiver (OVAR) (Fig. 1a), usually made of a ceramic or metal. The designed OVAR consists of cylindrical absorbers with circular porous and is made of brass (Fig. 1b). The thermal conductivity of brass is comparable to that of Silicon-carbide (SiC) in the considered temperature range. For more details refer to Sharma et al., 2015a, 2015b. Ambient air is heated to a high temperature as it flows through the circular pores. This unsteady process, eventually, leads to the desired steady state for given boundary conditions. Thus, to operate any process heat system based on such a receiver it is necessary to model the involved unsteady heat transfer process. For this purpose, both numerical and experimental evaluation of the designed circular pore based cylindrical absorber is presented in this section. The objective is to (a) develop an analysis tool and (b) understanding of the transient heat transfer process.

2.1 Mathematical model and numerical approach

For numerical analysis of a circular pore cylindrical absorber, the heat transfer process in porous absorber is mathematically modeled. The absorber is made of brass having thermal conductivity K_s~138W/mK. The involved modes are shown in Fig. 1c, which considers one-dimensional axial heat transfer in the pores with radial heat loss to ambient via insulation. During this process, air heats up to a higher temperature. This hot-air is utilized in a furnace and cooled to a temperature T_{ra}, which is higher than T_a. This relatively warm air is returned to OVAR through six injection ports that are marked G in Fig. 1a. The returned air gains heat from the absorber via external forced convection. A part of this air mixes with ambient and sucked through the pores of absorber. Thus, a fraction of the transferred heat to return air is reused. The return air system is not modeled in the presented analysis. This is obvious from the provided insulation around porous absorber as depicted in Fig. 1c. Further, the developed mathematical model assumes (a) uniform heat flux on the absorber surface exposed to electrical heating (b) volumetric heating owing to high thermal conductivity of brass (c) air as an ideal gas. Thus, the model simplifies the system into a one-dimensional heat transfer in solid, fluid and insulation domains. It should be emphasized that such a comprehensive tool will allow the first level analysis of new absorber designs.

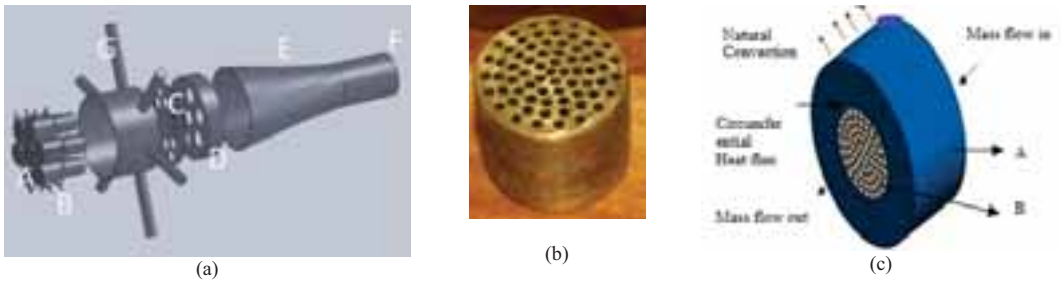

(a) (b) (c)

Fig. 1(a): Components of OVAR with A: Absorbers, B: Foot-piece, C: Anchor plate, D: mixer or perforated plate, E: Convergent nozzle, F: Outlet, G: Recirculating air injection ports, (b)Porous absorber of OVAR, (c) Porous absorber system model for numerical analysis with A:Insulation domain, B: Absorber(solid domain)

The model includes one-dimension conservation of energy equations in fluid, solid and insulation domains as in Eqn. 1-3. First-order explicit finite difference scheme is used for simultaneous l solution of the system of equations. Figure 2a and b depicts the control volume for fluid and solid domains. In the performed experiment Joule heating is applied to solid circumference of absorber that results in the desired volumetric heating. A small fraction of the input power conducted to the insulation and is finally lost to the ambient via natural convection (Fig 2d, e). The balance is transferred to ambient air via internal forced convection as shown Fig. 2b and c. The experimental parameters are presented in Table 1. The selected parameters are based on Sharma et al., 2015a and 2015b. The CFL condition (Anderson, 1995; Patankar, 1980) allows maximum time step of 0.13 ms for the considered final grid, which is obtained based on a grid dependence study. However, a smaller time step of 0.1 ms is selected for numerical heat transfer analysis. The length of absorber pore is 25.4 mm. The flow inside each pore is Laminar with Re ~ 102 and the corresponding Nusselt number for fully developed flow is 4.36 (Cengel, 2011; Incropera & DeWitt, 1996; White, 1998). However, the length of the absorber is of the order of its entry length, therefore, the Nusselt number for fully developed flow is modified using Eqn. 4, Subbarao, 2015.

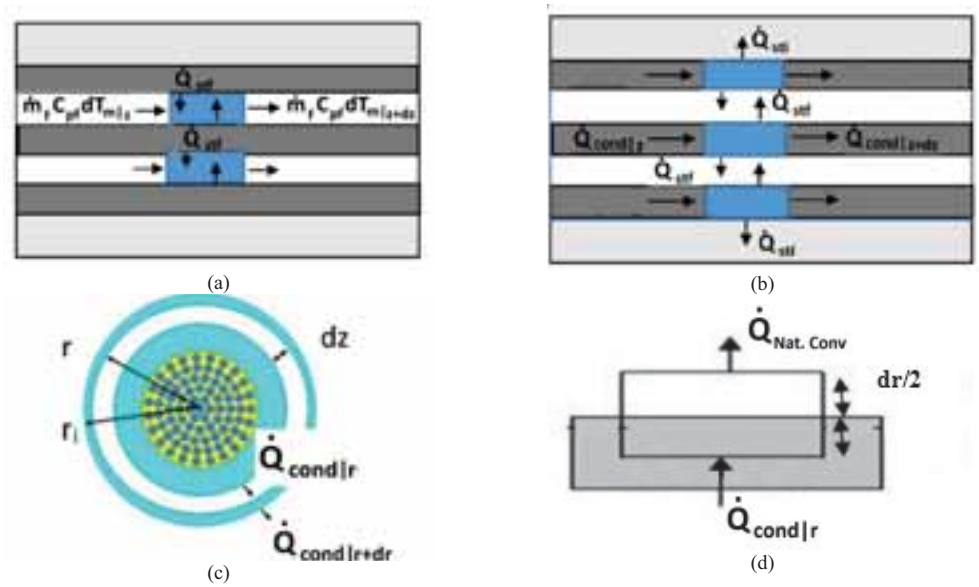

Figure 2: (a ,b)Control Volume for fluid and solid domain and (c, d) Control volume for insulation domain and its outer boundary condition

Solid:

$$\frac{\partial^2 T_s}{\partial z^2} - \frac{2h_f n_p r_p (T_s - T_m)}{K_s r_a^2 (1-\emptyset)} + \frac{2q''}{K_s r_a (1-\emptyset)} - \frac{2K_{ins}}{K_s r_a (1-\emptyset)} \frac{\partial T_{ins}}{\partial r}_{(r=r_a)} = \frac{1}{\alpha_s} \frac{\partial T_s}{\partial t} \quad \text{(eq. 1)}$$

Fluid:

$$\dot{m}_f \frac{\partial c_{pf} T_m}{\partial z} = 2\pi r_p n_p h_f (T_s - T_m) \quad \text{(eq. 2)}$$

Insulation:

$$\frac{\partial^2 T_{ins}}{\partial r^2} + \frac{1}{r} \frac{\partial T_{ins}}{\partial r} = \frac{1}{\alpha_{ins}} \frac{\partial T_{ins}}{\partial t} \quad \text{(eq. 3)}$$

The required heat transfer coefficient is estimated as follows:

$$Nu_f = 4.36 + \frac{0.086 (Re\ \mathrm{Pr} \frac{D}{L})^{133}}{1 + 0.1 Pr (Re \frac{D}{L})^{0.83}} \qquad 0.7 < \mathrm{Pr} < 7,\ \mathrm{Re} < 2300 \quad \text{(eq. 4)}$$

$$h_f = \frac{Nu_f k_f}{2r_p} \quad \text{(eq. 5)}$$

The initial and boundary conditions are as follows:

a. Initial condition: $T_{m.\ s.\ ins}(z = 0, t = 0) = 302.5K$
b. Inlet: $T_m(z = 0, t) = 305.7\mathrm{K}$, $\dot{m} = 0.00003\ kg/s$;
c. Insulated axial solid boundaries: $\frac{\partial T_s}{\partial z}\Big\}_{z=0.\ L\ and \forall t} = 0$
d. Solid-insulation interface: $T_s = T_{ins|r=r_s}$
e. External insulation surface: Natural convective heat loss is depicted as:

$$\frac{1}{r_{ins}} \frac{\partial T_{ins}}{\partial r}_{(r=r_{ins})} + \frac{h_{ex} (T_{ins_{(r=r_i)}} - T_a)}{K_{ins} r_{ins}} = \frac{1}{2\alpha_{ins}} \frac{\partial T_{ins}}{\partial t}_{(r=r_{ins})} \quad \text{(eq. 6)}$$

Where h_{ex} is calculated using the following correlation for natural convection:

$$Nu_{ex} = \left[0.6 + \frac{0.387 Ra^{1/6}}{\left[1 + (0.559/Pr)^{4/9}\right]^{8/27}} \right]^2 \quad \text{(eq. 7)}$$

$$h_{ex} = \frac{Nu_{ex} K_f}{2r_{ins}} \quad \text{(eq. 8)}$$

2.2 Experimental set-up

Experiment is performed for validation of the developed transient tool for heat transfer in porous absorber. The schematic of experimental set-up is shown in Fig. 3a. Air is blown into a steel pipe with outer diameter (D) of 25.4 mm and length (L) of 24D. At the outlet of pipe an absorber is fitted, which is electrically heated by externally wrapped Nichrome wire, see Fig. 2a & b. The experimental absorber is made of brass with porosity ~52 percent (83 pores of diameter (D_p)=2mm), length (L_a) and diameter (D_a) of 25.4 mm. Pipe and absorber are insulated using ceramic wool for reducing heat loss to ambient as shown in Fig. 3a and 3b. The input power is controlled by varying voltage using an auto-transformer and mass-flow-rate of air is maintained using a flow control valve. Temperature is measured using the calibrated K-type thermocouples with uncertainty of about 1-2%. Data from thermocouples is recorded and stored in real-time using NI-WSN gateway data acquisition (DAQ) device. The temperatures were measured at various azimuthal and radial positions as depicted in Fig. 3c at the inlet and outlet of the absorber.

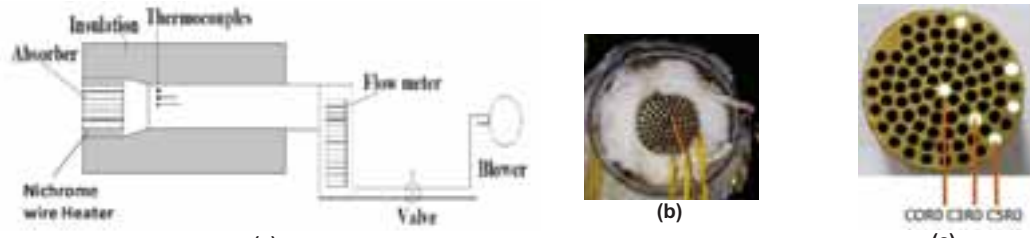

Figure 3: (a) Schematic of experiment set-up, (b): Front view of absorber with insulated , (c): Position of thermocouples on absorber

Table 1 shows the experimental parameters for the absorber. A part of the applied power to absorber is transferred to the connecting pipe via conduction. This heats up the air inside the pipe leading to an increase in temperature at the absorber inlet from 302.5 - 312K in 500 seconds. Thus, for validation of the developed numerical tool a time averaged inlet temperature of 305.7 K is used at the inlet. The net power input after subtracting the transfer to pipe as in Eqn. 9, is applied to absorber for this purpose. Thermocouples at various axial positions on the surface of insulation are mounted to estimate the rate of heat loss to ambient according to the second term on RHS of Eqn. 9. Also, thermocouples located on various radial positions at the pipe inlet and outlet are used to estimate mean air temperature at these positions, required for estimating the first term on RHS of Eqn. 9. An overall uncertainty of up-to 10% is attributed to (a) input power variation (b) temperature and mass flow rate measurements (c) manual operation and variable ambient conditions. Further, the numerical tool is designed to solve the equations with constant as well as variable fluid properties. For variable property the best fit curves are considered (Ekanayke, 2015; Boutelop, 2015). The properties of insulation and absorber materials are considered as constants. These are defined as average values in temperature range of 300-600K to cover the expected experimental conditions.

Tab. 1: Experimental and computational parameters for absorber

Parameter	Value	Parameter	Value
Mass Flow Rate	0.0003 *kg/s*	Power transfer to pipe ($\dot{P}$)	1.25 W
Reynolds Number	102	Net power input ($\dot{E}$- $\dot{P}$)	19.65 W
Current	1.95 $\pm$0.05A	T_{inlet}	302.5 – 312 K
Resistance	5.5 $\pm$0.1 Ω	$T_{inlet,\ time\ averaged}$	305.7 K
Electrical Power Input ($\dot{E}$)	20.9 W	Equivalent Radiative Heat Flux	20 kW/m2
Effective POA/MFR	65.5 kW/kg/s	Equivalent concentration (suns)	80 Suns
$K_{s,avg.}$	138.7W/mK	$Cp_{s,\ avg}$	0.413 kJ/kgK
$\alpha_{f,\ avg}$	19.9 m^2/s	$Cp_{f,\ avg}$	1.009 kJ/kgK

$$\dot{Q}_{atp} = \dot{m}_f c_{pf,}\left(T_{m,pipe\ outlet} - T_{m,pipe\ inlet}\right) + \Sigma h_{ex} 2\pi r_{ins} \Delta l (T_{ins} - T_a) \qquad \text{(eq. 9)}$$

2.3 Results

Figure 4a shows the transient variation of temperature in pores located at different radial positions as shown in Fig. 3c. It is observed that the temperature development is practically comparable at all these three locations with a variation of about ±1˚C. This confirms the assumption that heat is uniformly distributed throughout the solid and that the bulk fluid temperature is, practically, comparable. This situation will be different including air return system in which radial variation of fluid temperature is expected as shown in Sharma et al., 2015a, 2015b. Thus the code will be extended in the near future including this effect as well. A

comparison between the numerically analyzed bulk-mean and measured air temperature with respect to time is shown in Fig. 4b. The maximum difference of ~ 10% is observed between these values. For simulation both constant and temperature dependent air properties are used. Thus, it can be safely stated that such a tool will be extremely useful for predicting unsteady heat transfer process in absorber for process heat application.

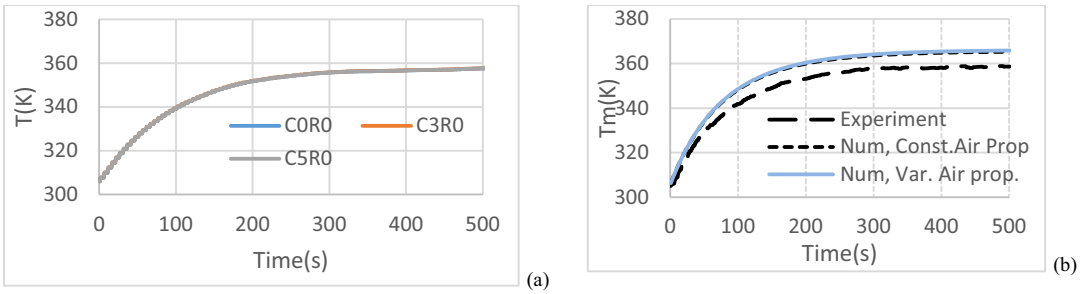

Figure 4 : (a)Variation in temperature between different absorber pores as observed in the experiment (b): Comparison between 1-D and measured bulk-mean air temperature with time

3. Heat transfer in an insulated pipe

As described, hot air is transported in an insulated pipe to thermal energy storage for its use in, for example, solar convective furnace to achieve steady state. Attaining the desired steady state will be influenced by (a) heating up of the piping network and (b) heat loss to ambient via insulation from hot air. Thus, understanding and development of a transient analysis tool will support the operation of such a system. For this purpose, a one-dimensional heat transfer model is developed and validated with the performed experiment under the same conditions.

3.1 Numerical approach

For the development of one-dimensional tool, the insulated piping system with air-flow is represented using three domains, namely, fluid (air), solid (pipe) and insulation. The control volumes for each domain are shown in Fig. 5a, b and d. The derived energy equations in each domain are solved, simultaneously, using a numerical scheme. The hot fluid entering the pipe loses heat to the solid (pipe material) and finally to ambient via insulation with external natural convection. Further, the solid domain loses heat to the ambient via natural convection at its axial boundary ($z=0, L$), the control volume of which is shown in Fig. 5c. For fluid domain, instantaneous mass-weighted average temperature equation is derived ignoring storage as heat is convected. For the solid domain, the conduction in the radial direction is neglected considering small pipe thickness in comparison to the pipe length. For insulation domain, heat transfer in radial direction is considered on account of a lower thermal resistance at its radial boundary in comparison to axial boundary as a result of higher surface area for convective losses.

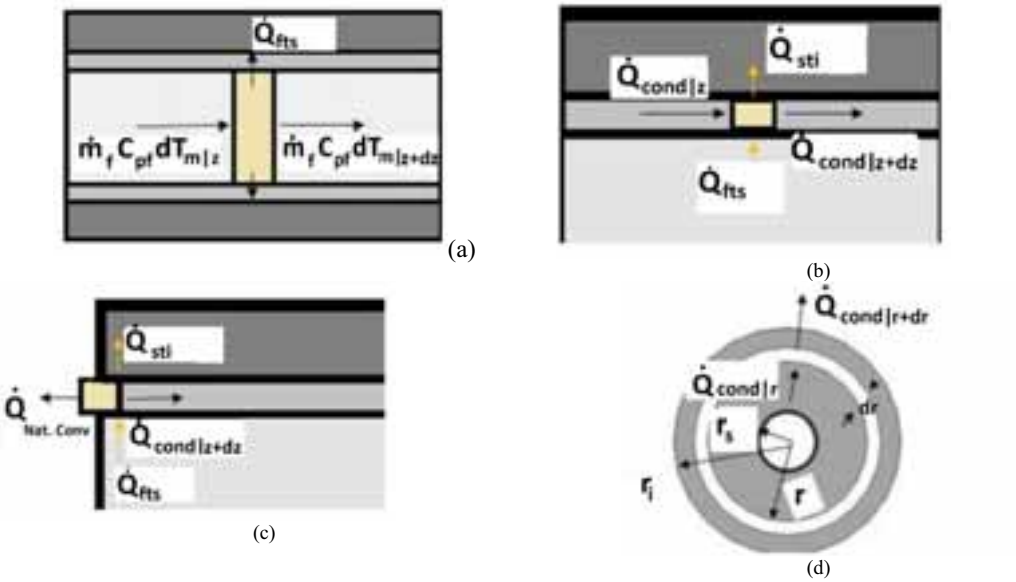

Figure 5 (a, b, d): Control volume of fluid, solid and insulation domain, (c): Control Volume for boundary conditions(z=0,L) for solid domain

Energy equations in solid (pipe), fluid and insulation domains are given by Eqn. 10, 11 and 12, respectively. The partial differential equations are solved with first-order accuracy. Explicit forward-difference-scheme with uniformly spaced grid points in fluid and solid pipe domain is employed for discretization. Corresponding CFL conditions (Patankar, 1980; Anderson, 1995) are satisfied in each domain for the considered mesh sizes and time steps. Average values of material properties, like thermal conductivity, density, viscosity, etc. in the temperature range was considered and assumed to be constant. This is acceptable for the performed experiment with limited temperature range. However, the tool will be generalized with variable fluid properties at the next step, once validated.

Solid (Pipe) Domain:

$$\frac{\partial^2 T_s}{\partial z^2} + \frac{h_f(T_m - T_s)}{K_s \delta} + \frac{K_{ins}}{K_s \delta}\frac{\partial T_{ins}}{\partial r}_{(r=r_s+\delta)} = \frac{1}{\alpha_s}\frac{\partial T_s}{\partial t} \quad \text{(eq. 10)}$$

Fluid Domain (instantaneous):

$$\frac{\partial T_m}{\partial z} = -\left(\frac{2\pi r_s h_f}{\dot{m}_f c_{pf}}\right)(T_m - T_s) \quad \text{(eq. 11)}$$

Insulation:

$$\frac{\partial^2 T_{ins}}{\partial r^2} + \frac{1}{r}\frac{\partial T_{ins}}{\partial r} = \frac{1}{\alpha_{ins}}\frac{\partial T_{ins}}{\partial t} \quad \text{(eq. 12)}$$

The boundary and initial conditions are as follows:

a. The inlet temp of fluid : $T_m(z = 0, t) = 400\text{K}$
b. Initially the solid pipe and insulation domain are at ambient temperature:
   $\therefore T_s(z, t = 0) = T_{amb} = T_{ins}(r, z, t = 0)$
c. Natural convection boundary condition at axial boundaries for solid domain i.e. z=0 and z=l represented by equation 10.

$$\frac{\partial}{dz}\left[(-1)^n (K_s 2\pi r\delta)\frac{\partial T_s}{dz}\right]_{z=0,L} + h_f 2\pi r(T_m - T_s) + K_{ins} 2\pi r \frac{\partial T_{ins}}{dr}_{(r=r_s+\delta)} + h_{ex} 2\pi r\delta(T_s - T_a) = 2\pi r(\delta)\rho_s C_{ps}\frac{\partial T_s}{dt} \quad \text{(eq. 13)}$$

Here, n= 1 if z=0 & n= 2 if z= L and h_{ex} is estimated using the following Nu correlation

d. Natural convection boundary condition at radial boundary of the insulation domain while axial boundaries are assumed to be insulated similar to absorber as shown in Eqn. 6

Dittus-Boelter correlation (Cengel, 2011) for internal air-flow is used for estimation of heat transfer coefficient in fully developed region as in Eqn. 14. This is modified in the entry length region using Eqn. 15. Natural convection based heat loss coefficient to ambient from the exposed solid and insulation surfaces is estimated through Rayleigh number using Eqn. 17. Equations 16 and 18 represent the heat transfer coefficient relationship with corresponding Nusselt no and characteristic length for internal and external flow respectively.

$$Nu_{f,fd} = 0.027 * Re^{0.8} Pr^{\frac{1}{3}} \quad \text{(eq. 14)}$$

$$\frac{Nu_f}{Nu_{f,fd}} = \left(\frac{x}{2r_s}\right)^{-0.0054} \quad \text{(eq. 15)}$$

$$h_f = \frac{Nu_f k_f}{2r_s} \quad \text{(eq. 16)}$$

$$Nu_{ex} = \left[0.6 + \frac{0.387Ra^{1/6}}{\left[1+\left(^{0.559}/_{Pr}\right)^{4/9}\right]^{8/27}}\right]^2 \quad \text{(eq. 17)}$$

$$h_{ex} = \frac{Nu_{ex} k_f}{2\delta} \quad \text{(eq. 18)}$$

3.2 Experimental set-up

The designed and installed experimental set-up and its schematic are shown in Fig. 6a & 6b. In this experiment, to achieve a constant high temperature at the pipe inlet (*z=0)*, a heating element is designed. Heating element is a separate steel-pipe of 25.4 mm diameter in which three porous bodies (absorbers) are fitted at different axial locations. Their purpose is to allow effective heat transfer to air as well as thermal mixing. A Nichrome wire of 0.25 mm diameter is wrapped on external pipe surface for additional Joule heating. Needless to say, the porous bodies will introduce extra pressure drop, which is not of primary concern for the present purpose. Thus, in experiments, at the outlet of heating element air stream at uniform temperature is obtained. It requires sometime to achieve the steady value in the heating element. Therefore, it is bypassed through a valve into atmosphere. Once the steady air temperature is reached the inlet valve of main pipe is opened and atmospheric bypass valve is closed. In this way at the main pipe inlet of 53.6 mm diameter a constant temperature boundary condition is maintained throughout the experiment. Calibrated thermocouples are mounted inside and on the surface of 0.7 m long insulated main pipe at several axial and radial positions, see Fig. 6c. Temperature of pipe and insulation is also recorded using NI DAQ device. Table 2 presents the input parameters for the experiment conducted for code validation. For a fixed mass flow rate inlet, hot wire anemometer was used to measure the velocity at a reference temperature of 30 ˚C. Radius of Insulation greater than the critical radius of insulation (~53.6 mm) was chosen for validation (Incropera, 1996; White, 1998; Holman, 1997). An uncertainty of ~5-10% is attributed to fluctuations in ambient temperature, power and error in measuring the temperature via thermocouples.

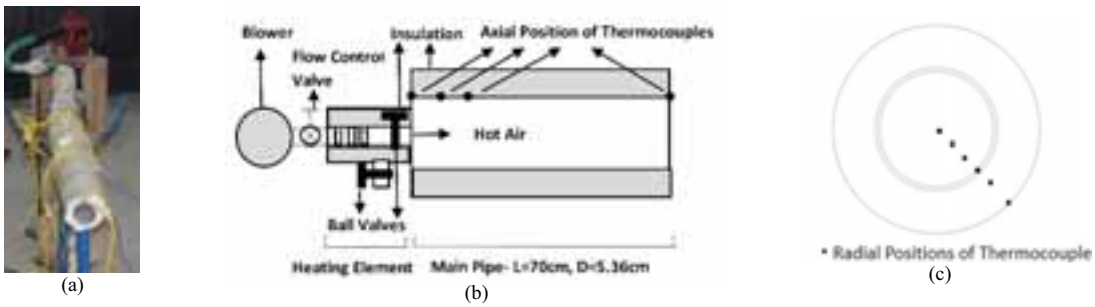

(a) (b) (c)

Figure 6: (a, b) Experimental set-up and its schematic; (c) Position of Thermocouples

Tab. 2: Experiment Input Parameters for pipe

Parameter	Value
Avg. Mass Flow Rate	0.005 kg/s
Velocity	2.2 ±0.1m/s at 304K
Current for electrically heating the absorbers	3.15 ±0.05A
Resistance	62.5 ±0.1 ohm
Reynolds Number	4707
$T_{m \text{ at } z=0}$	400± 2 K
$T_{S \text{ at } z=0=t}$	314± 1 K

3.3 Results

Constant air temperature boundary condition at the main-pipe inlet ($T_{m \text{ at } z=0}$ = 400 K) with mass flow rate of ~0.005 kg/s is imposed on in both experiment and numerical analysis. A comparison between unsteady heat transfer experiment and 1-D numerical analyzed data for hot-air flow in the insulated pipe is shown in Fig. 7a, b and c. These are for bulk or mean temperature of air, solid (pipe) at the outlet and for insulation at the inlet and outlet over time. Generally, higher air temperatures are estimated numerically in comparison to experiment. The temperature differences of solid at the pipe inlet and outlet in Fig. 7b indicate a better correlation for heat loss is required within the thermal entry length. However, the general trend of temperature development is captured adequately. Figure 7c depicts that the code under-predicts the losses to the ambient as a result of under-prediction of insulation temperature. This is consistent with the over-predicted temperatures of solid and fluid at the outlet. The maximum differences between numerically and experimentally obtained values are ~5-15%. Therefore, it is expected that this tool will be helpful in analyzing and predicting unsteady heat transfer in a piping network for furnace system. (Patidar et al, 201b).

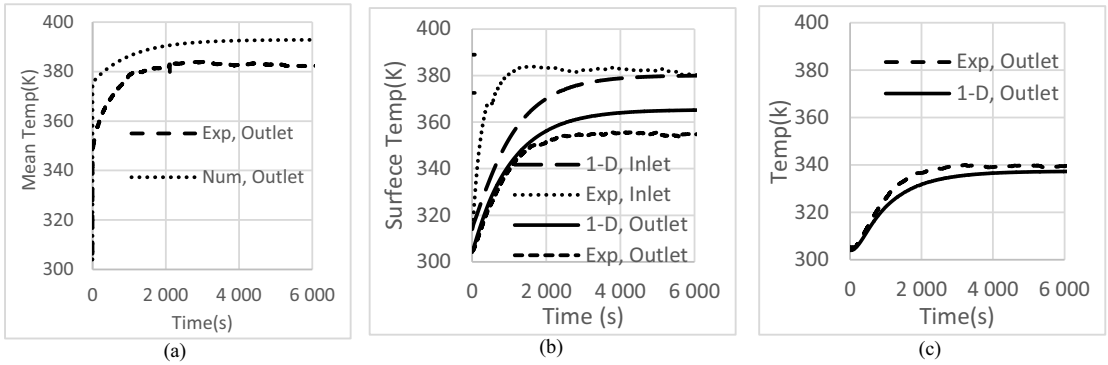

Fig7: Comparison between 1-D analysis and experiment for fluid (a), solid pipe (b) and insulation (c) domains.

4. Conclusion

The paper deals with the development of validated mathematical models for unsteady heat transfer analysis in a porous absorber and of an insulated pipe. These are sub-systems for a solar convective furnace. The developed tool has its application in designing receiver and piping network of a solar convective furnace system. For developing this system level tool one-dimensional modeling approach of the considered sub-systems/components, like, porous absorber and insulated pipe is considered. For solving these equations a first-order accurate explicit numerical scheme is utilized. Experiments are performed for validation of the adopted model and numerical method. The comparison between experiment and numerically analyzed data, namely, air, solid and insulation temperatures reveal a variation of about 5-15%. This is expected as the modeling is limited to one-dimension and utilizes simplified experimental correlations. However, even with these known limitations, it can be safely stated that such a tool will be extremely valuable in predicting performance of the desired solar convective furnace system.

5. References

Anderson Jr., J. D., 1995. Computational fluid dynamics: the basics with applications, McGraw Hill Inc.

Bouteloup P., 2015 September 1, http://bouteloup.pierre.free.fr/lica/phythe/don/air/air_nu_plot.pdf

Cengel Y.A., 2011. Heat and Mass Transfer, Fourth Edition, McGraw Hill Inc.

Hoffschmidt B., Téllez F. M., Valverde A., Fernández J., Fernández V., 2003. Performance evaluation of the 200-kWth HiTREC-II open volumetric air receiver. Journal of Solar Energy Engineering, 125, pp. 87–94.

Holman J.P., 1997. Heat Transfer, eighth ed., McGraw-Hill Publishers, New York, pp. 38–39.

Ekanayke P. 2015 September 1. ninova.itu.edu.tr/tr/dersler/ucak-uzay-fakultesi/965/uck.../ekkaynaklar

Incropera F.P., DeWitt D.P., 1996. Introduction to heat transfer, third ed., John Wiley Publ., New York, pp. 93–99.

Material Properties, 2015 September 1, http://www.engineeringtoolbox.com

Patankar S.V., 1980. Numerical Heat Transfer and Fluid Flow, McGraw Hill Book Company

Patidar D., Tiwari S, Sharma P, Chandra L, Shekhar R, 2015a. Open volumetric air receiver based solar convective aluminum heat treatment furnace system, Energy Proc. 69, pp. 506-517.

Patidar D., Tiwari S., Sharma P., Pardeshi R., Chandra L., Shekhar R., 2015b. Solar convective furnace for metals processing, JOM, pp. 9 pages, DOI: 10.1007/s11837-015-1633-z.

Sharma P., Sarma R., Chandra L., Shekhar R., Ghoshdastidar P. S., 2015a. Solar tower based aluminum heat treatment system: Part I. Design and evaluation of an open volumetric air receiver, Solar Energy, 211, pp. 135-150.

Sharma P., Sarma R., Chandra L., Shekhar R., Ghoshdastidar P. S., 2015b. On the design and evaluation of open volumetric air receiver for process heat applications, Solar Energy, doi:10.1016/j.solener.2015.05.027.

Subbarao P.M., 2015 September 1,http://web.iitd.ac.in/~pmvs/courses/mel242/mel242-27.ppt

Vasiliev L.L, Kiselev V. G, Matveev Yu N., Molodkin F.F., 1987 Heat Pipe Heat Exchangers, Nauka Technica, Minsk, (in Russian).

White F M, 1998.Fluid Mechanics, Fourth Edition, WCB McGraw-Hill